Vibration Suppression With Shaft Torque Limitation Using Explicit MPC-PI Switching Control in Elastic Drive Systems

Can Wang, Ming Yang, *Member, IEEE*, Weilong Zheng, Jiang Long, and Dianguo Xu, *Senior Member, IEEE*

***Abstract*—In this paper, the application of model predictive control (MPC) for torsional vibration suppression and shaft torque limitation control in the elastic drive system is demonstrated. Standard MPC is converted to fast explicit MPC (EMPC) to solve its difficult online implementation issues. Constraint condition of shaft torque limitation control is first proposed through theoretical derivation, implying that the responses of shaft torque vary with the changed critical value of shaft torque, but the limitation function can still be available. Eventually, the EMPC-PI switching control is used for the application of shaft torque limitation control into the typical drive successfully, which can significantly reduce the amount of data storage, closer to practical industrial applications. Meanwhile, the advantage of eliminating the steady-state error provided from the PI controller can further enhance robustness of the system, compared with the pure EMPC controller. The switching criterion is based on the speed hysteresis value, which can be properly adjusted under different circumstances. Simulation and experimental results of speed step responses verify the EMPC-PI switching controller as a more effective approach compared with the PI controller designed by pole-placement method.**

***Index Terms*—Constraint condition of shaft torque limitation control, drive system, explicit MPC (EMPC)-PI switching control, mechanical resonance, model predictive control (MPC).**

I. Introduction

MODERN industrial drives are required to present relatively high dynamic properties. However, torsional vibration caused by elastic transmissions affects the drive system performance significantly [1]. The torsional characteristics of the mechanical coupling lead to the increasing of angular vibrations of the shaft. Excessive shaft twists and poorly damped torsional vibrations will beyond the shaft' s tolerance, which may lead to the risk of poor system performance, and system instability, and in some cases, the accident such as shaft breaking will occur [2].

In an attempt to overcome these challenges, there are a number of proposals have been developed that can be divided into two categories: passive and active. Passive mode refers to the application of the notch filter [3]; Active mode can be categorized into basic PI control (two degrees of freedom PI control, RRC [4]), state feedback control based on PI, and other advanced algorithms [5].

The most popular classical method is PI control in the speed loop. Various design approaches for tuning the PI parameters have been reported [6]. These algorithms are simple, well established, and accepted by industry. However for the constricted poles' location of the closed-loop system, this method fails to shape the system response and suppress the torsional oscillations simultaneously.

In order to improve system's response to the state variables, based on a suitable location of the closed-loop system poles, the application of the feedback from the corresponding state variable is necessary. As shown in [7], the inclusion of one additional feedback (the estimated shaft torque) is proposed. Using motor acceleration, this method is commonly referred to as resonance ratio control (RRC). However, in this case, the settling time of the step response cannot be set randomly by choice of the feedback gains, and better results can be obtained using all system feedback variables [8]. Still, the direct feedback from these signals are often impossible because of the difficult and costly measurements, which need more state observers of immeasurable variables [9].

In spite of the successful vibration suppression of the state feedback method, the authors acknowledge the loss of dynamic performance. More sophisticated control paradigms can be adopted to allow a free pole placement of the closed-loop control and, thus, a theoretically free choice of the system dynamics, but they are not yet popular in industrial applications [10]. The application of the sliding or the fuzzy control [11] increases the robustness of the drive system to parameter variations. A strategy based on a self-tuning regulator and nonlinear Kalman filter is proposed in [12]. A robust predictive patch is proposed in [13], [14] to ensure system's safety. The essence of this patch is to calculate the maximum robust control set of variables within the scope of allowable state variables. With the patch, all the existing physical and safe limits of the states are realized.

Manuscript received October 28, 2014; revised March 7, 2015; accepted April 16, 2015. Date of publication June 1, 2015; date of current version October 7, 2015. This work was supported in part by the Research Fund for the National Science Foundation of China under Grant 61273147 and in part by grants from the Power Electronics Science and Education Development Program of Delta Environmental and Educational Foundation under DREK2012002.

The authors are with the School of Electrical Engineering and Automation, Harbin Institute of Technology, Harbin 150001, China (e-mail: yangming_hit@163.com).

Color versions of one or more of the figures in this paper are available online at http://ieeexplore.ieee.org.

Digital Object Identifier 10.1109/TIE.2015.2438055

The most commonly used method to deal with bounds on the state variables in control system is MPC [15], [16]. MPC methodology relies on incorporating the drive's safety and physical limitations as the control objectives directly into the control problem formulation so that future constraint violations are anticipated and prevented. In order to reduce the amount of online computation, the standard MPC controller is simplified as its explicit form [17]. The resulting explicit MPC (EMPC) controller achieves the same level of performance as the conventional MPC, but requires only a fraction of the real-time computation, thus leading to fast and reliable implementation. As shown in [18] and [19], EMPC is used as the speed and position loop controller, respectively, directly outputting the optimal electromagnetic torque to achieve limitation control of the speed, shaft torque and electromagnetic torque. In [20], the constraints of the current and voltage in the controller are enforced with EMPC. The novelty exists in adding an integrator of the angular speed error outside of the controller, to solve the typical problem of MPC dealing with unmeasured disturbances and parameter mismatch. Also, a low-pass filter in the speed feedback is introduced not only to filter out high-frequency noise coming from the resolver/encoder or to account for some unavoidable effects like time delays in the measurement.

In [21], it is shown that the variation of the system parameters does not weaken the ability of the MPC controller to handle the physical and safety constraints of the drive during operation. However the MPC control structure is not so robust with respect to the shape of drive speed transients. Kalman filter is employed to observe the system states in the EMPC system [21]–[23], which can increase the robustness of the drive system against plant parameter variations such as the natural angular frequency of the system, the load inertia, shaft stiffness, electromagnetic torque and shaft torque. A robust MPC controller is designed with suitable selection of the elements of the covariance matrices Q and R in speed loop and position loop, respectively [24], [25]. The methods are Generalized Pattern Search and Genetic Algorithm. They all concluded that the shapes of the load speeds for different values of load machine are almost identical. In addition, the set control constraints of the shaft torque are not validated.

In spite of the amount of EMPC online computation that can be reduced, due to its high requirements for the control module memory, EMPC applications to electrical drives are still largely constricted [26]. Rapid control prototype such as dSPACE 1104 HIL system is still needed in all the EMPC-controlled practical applications aforementioned, to make the algorithm successfully implemented in the real systems [18]–[25]. This method applies upper computer to control the hardware platform directly, making it impossible for the simple implementation in the typical drive, which has brought a lot of limitations for the application in industrial conditions.

There are two novelties in this paper: the first one is the proposal and verification of the constraints for shaft torque limitation for the first time. There existed a shaft torque amplitude limitation critical value, when the preset shaft torque limiting value $\overline{T}_s$ is less than or equal to this critical value, the shaft torque will output its preset value during the system operation; when $\overline{T}_s$ is bigger than the critical value, the shaft torque will oscillate. The second contribution of this paper is the realization of EMPC-PI switching control with no requirements for advanced hardware platform which can be applied in real typical drives and further enhanced the practical application of prediction algorithm.

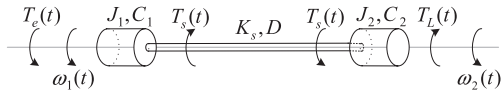

Fig. 1. Schematic of the two-mass elastic system.

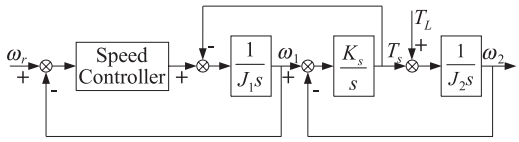

Fig. 2. Block diagram of the two-mass elastic system.

This paper mainly deals with the mechanical resonance and system safety problems in the two-mass system with an elastic coupling. It is organized as follows. The mathematical model of the drive system is analyzed in Section II, and then the algorithm is simplified to design the EMPC controller to solve the online implementation issue in Section III. Section IV makes the main contribution of theoretical derivation of the constraints for shaft torque limitation control. In Section V, the novel EMPC-PI switching control is investigated, which is successfully implanted in the PMSM drive system. Simulation and experimental results confirm that the controller can guarantee both dynamic performance and safety of the system.

II. Model of the Two-Mass Elastic System

In many cases, the drive system can be simplified to a two-mass motor/load system with an elastic coupling. The mechanical coupling is treated as inertia free. So the drive system under consideration is schematically shown in Fig. 1.

In this schematic, the motor and actuator are coupled by the transmission system with finite stiffness K_s and internal damping D. When the shaft torsional deformation exists, the shaft will generate a torsional torque T_s, which is affected by the angle difference between the motor and actuator, as well as the mechanical damping. Electromagnetic torque T_e and shaft (torsional) torque T_s act together on the motor (the moment of inertia J_1, damping coefficient C_1). On the other hand, T_s and load torque T_L work together on the actuator (the moment of inertia J_2, damping coefficient C_2), deciding its speed.

Based on the theoretical analyses aforementioned, the system is described by the following differential equations:

$$\begin{cases} J_1\ddot{\theta}_1 = T_e - C_1\dot{\theta}_1 - T_s \\ J_2\ddot{\theta}_2 = T_s - C_2\dot{\theta}_2 - T_L \\ T_s = D(\dot{\theta}_1 - \dot{\theta}_2) + K_s(\theta_1 - \theta_2) \\ \omega_1 = \dot{\theta}_1 \\ \omega_2 = \dot{\theta}_2. \end{cases} \tag{1}$$

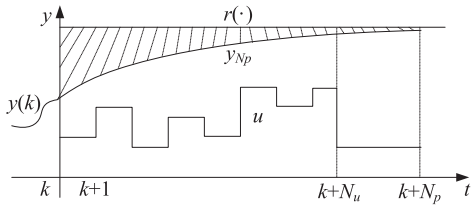

Fig. 3. Schematic of MPC.

Since frictional effect is usually considered to be relatively small in most industrial systems, by putting $C_1 = C_2 = 0$ in Fig. 2, the block diagram of the mechanical model is obtained.

III. Vibration Suppression and Shaft Torque Limitation Control Based on MPC

MPC is also known as receding horizon control, dynamic matrix control and generalized predictive control. It is also a feedback control strategy, which has been widely discussed in recent years.

Originating from industry, predictive control intends to solve constrained optimization of multivariable control problems which are not easy to be implemented with PID control. Theoretically, MPC can handle constrained optimal control problems in time-varying or time-invariant, linear or nonlinear, time-delay or nondelay systems, which has made it a very effective method.

A. Principle of MPC

As shown in Fig. 3, at the moment of k, the measured output $y(k)$ is obtained from the control system. Meanwhile, a dynamic model is applied to predict future response of the system. The state-space model is used as an example.

MPC design requires a discrete-time model for a correct approximation of the fastest dynamics to predict the evolution of the system. The state-space form is described in

$$\begin{aligned} x(k+1) &= Ax(k) + Bu(k) \\ y(k) &= Cx(k) \end{aligned} \tag{2}$$

where $x(k)$, $u(k)$, and $y(k)$ denote the state, input, and output variables, respectively. Since (2) is a difference equation, $x(k)$ is needed as the starting point of predictive state in calculation and is estimated by a state observer

$$\begin{aligned} J\left(x(k), U_k\right) &= \sum_{i=k+1}^{k+N_p} \left(r(i) - y_{N_p}(i|k)\right)^2 \\ &= \sum_{i=0}^{N_p} x_{k+i|k}^T Q x_{k+i|k} + \sum_{i=0}^{N_u-1} u_{k+i}^T R u_{k+i}. \end{aligned} \tag{3}$$

The purpose of the control is to find the optimal control input, to make the system output y_{Np} follow the desired output, i.e., the reference input $\{r(k+1), r(k+2), \ldots, r(k+N_p)\}$. For this purpose, a simple formulation of optimal cost function is expressed by the cumulative error, which is described as (3), where Q and R are positive-definite weighting matrices, N_p and N_u denote the prediction and control horizons, respectively. In addition, control input $U_k = \{u(k|k), u(k+1|k), \ldots, u(k+N_u-1|k)\}$ is exactly the independent variable to be solved in the optimization problem. In other words, the aim of the control strategy is to decrease the area of the shaded part in Fig. 3 to the biggest extend, whereas satisfying the system constraints of outputs and inputs

$$\begin{aligned} u_{\min} \le u(k+i) \le u_{\max}, \quad i \ge 0 \\ y_{\min} \le y(k+i) \le y_{\max}, \quad i \ge 0. \end{aligned} \tag{4}$$

Then, the aforementioned question can be described as the following optimal control problem:

$$\text{Question 1} \quad \min_{U_k} J\left(x(k), U_k\right).$$

Thus, the basic principle of MPC can be summarized as follows: At each time step k, the latest obtained measurements are used to refresh optimization Question 1, that is the MPC controller chooses the best control input signal to optimize future plant behavior while respecting the system input/output constraints by minimizing the given cost function. Once the optimal input sequence has been computed, only the first sample will be applied to the physical system.

Substituting $x = Ax_{k|k} + BU$ into (3), the MPC problem can be solved by the quadratic programming

$$\begin{aligned} V\left(x(k)\right) &= x(k)^T Y x(k) + \min_U \left\{U^T H U + 2x(k)^T F U\right\} \\ \text{subject to} \quad & GU \le W + Ex(k) \end{aligned} \tag{5}$$

where $H = B^T Q B + R$, $F = A^T Q B$, $Y = A^T Q A$.

The implementation of the MPC controller amounts to solving (5) online in a receding horizon fashion. However, the computational effort should be taken into consideration when applying MPC into practice. EMPC offers a way to systematically subdivide the parameter space into polyhedral regions and obtain the associated affine control law as a kind of offline computation form, where the optimizer is given as a piecewise affine (PWA) function, which can significantly reduce the online calculation time.

Introducing $z = U + H^{-1}F^T x(k)$, optimization problem (5) can be transformed into the following form:

$$\begin{aligned} V\left(x(k)\right) &= \min_z z^T H z \\ \text{subject to} \quad & Gz \le W + Sx(k) \end{aligned} \tag{6}$$

where $S = E + GH^{-1}F^T$. Indeed, in the case of a linear system with constraints and a quadratic cost function of the state, the optimization problem suits KKT conditions [21] combined with active set method for solving a multiparametric quadratic program. In particular, the multiparametric toolbox (MPT) for Matlab is efficient enough to solve the optimization problem, where the explicit lookup table is automatically generated, leading to faster and more reliable implementation.

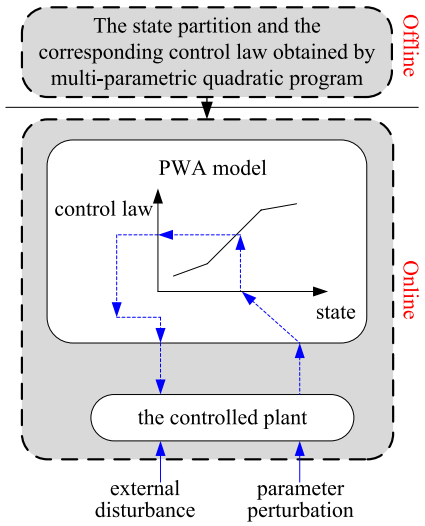

Fig. 4. Online and offline computation process of EMPC.

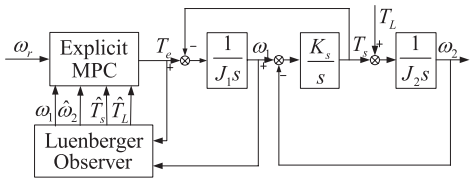

Fig. 5. Two-mass drive system control structure with the EMPC controller.

In each region of the state space, the control law can be expressed as the following form, and then the optimal control solution is obtained with a small amount of computation:

$$u_i(k) = F_i x(k) + G_i \tag{7}$$

where i is the index of the region and the matrices F_i and G_i are the results of the optimization algorithm described in (6).

Fig. 4 shows the whole computation process of the EMPC system, making it possible to execute the algorithm fast enough to fit the typical electrical drives.

B. EMPC Design Based on the Two-Mass Elastic System

This section outlines the procedure for designing the EMPC law for the considered two-mass drive system, which can achieve better vibration suppression and shaft torque limitation. The block diagram of the overall control structure incorporating the EMPC controller is schematically shown in Fig. 5.

The Luenberger state observer is designed by the pole placement method. After verifying the observable of the system, on the basis of recursion formulas of Luenberger state observer, the pole of the observer is assigned as 0.8, which enables a stronger antidisturbance ability of the observer and finally gains the feedback gain matrix.

For the purpose of obtaining the EMPC control law and satisfying the requirements of system constraints, all the parameters that affect the result of the optimization, such as the reference speed ω_r and the load disturbance T_L must generally explicitly be part of the controller states, which can be achieved by defining the following augmented model:

$$\begin{bmatrix} \dot{\omega}_1 \\ \dot{\omega}_2 \\ \dot{T}_s \\ \dot{T}_L \\ \dot{\omega}_r \end{bmatrix} = \begin{bmatrix} 0 & 0 & -J_1 & 0 & 0 \\ 0 & 0 & J_2 & -J_2 & 0 \\ K_s & -K_s & 0 & 0 & 0 \\ 0 & 0 & 0 & 0 & 0 \\ 0 & 0 & 0 & 0 & 0 \end{bmatrix} \begin{bmatrix} \omega_1 \\ \omega_2 \\ T_s \\ T_L \\ \omega_r \end{bmatrix} + \begin{bmatrix} J_1 \\ 0 \\ 0 \\ 0 \\ 0 \end{bmatrix} T_e. \tag{8}$$

Then, EMPC law is designed according to the required optimization objective to achieve better dynamic performance and transmission safety. In order to prevent the produced motor torque from exceeding its maximum allowable value, the following physical constraint is introduced, where $\overline{T}_e$ incorporates the physical limit of the drive power converter:

$$|T_e| \le \overline{T}_e. \tag{9}$$

A critically important requirement for drive's safety and long-term reliable operation is to prevent excessive shaft twists which may occur during the drive transients. In principle, the maximum torsional stress values undertaken by a shaft must be considerably smaller than the ultimate tensile stress limit of the shaft and less than the yield stress limit of the material. This is addressed by imposing the safety constraint

$$|T_s| \le \overline{T}_s. \tag{10}$$

In this paper, $\overline{T}_s$ is used as a design parameter to demonstrate the constraint handling capability of the proposed EMPC and to study its impact on the closed-loop performance.

To solve the constraint problem the system required, N_p and N_u should be properly selected. Ideally, it has to be chosen long enough to include the most relevant part of the system. Unfortunately, large prediction horizons might unavoidably require a large number of control moves to be available in the controller, thus greatly impacting on the computational complexity of the algorithm. In this paper, the state variables are predicted using a 7 ms prediction window and the control input is calculated over 0.5 ms intervals. The control horizon N_u, which is the number of steps after which the input signal is considered steady when predicting the future response of the system, is set to be 3

$$N_p = 14 \quad N_u = 3. \tag{11}$$

The proper selection of cost function is of great importance to the system performance. In this context, in the order of importance according to the target, the speed reference tracking error should be penalized more heavily than the error caused by the shaft-load torque imbalance, which can be addressed by defining the following error variables:

$$\begin{aligned} y_1 &= \omega_1 - \omega_r \\ y_2 &= T_s - T_L. \end{aligned} \tag{12}$$

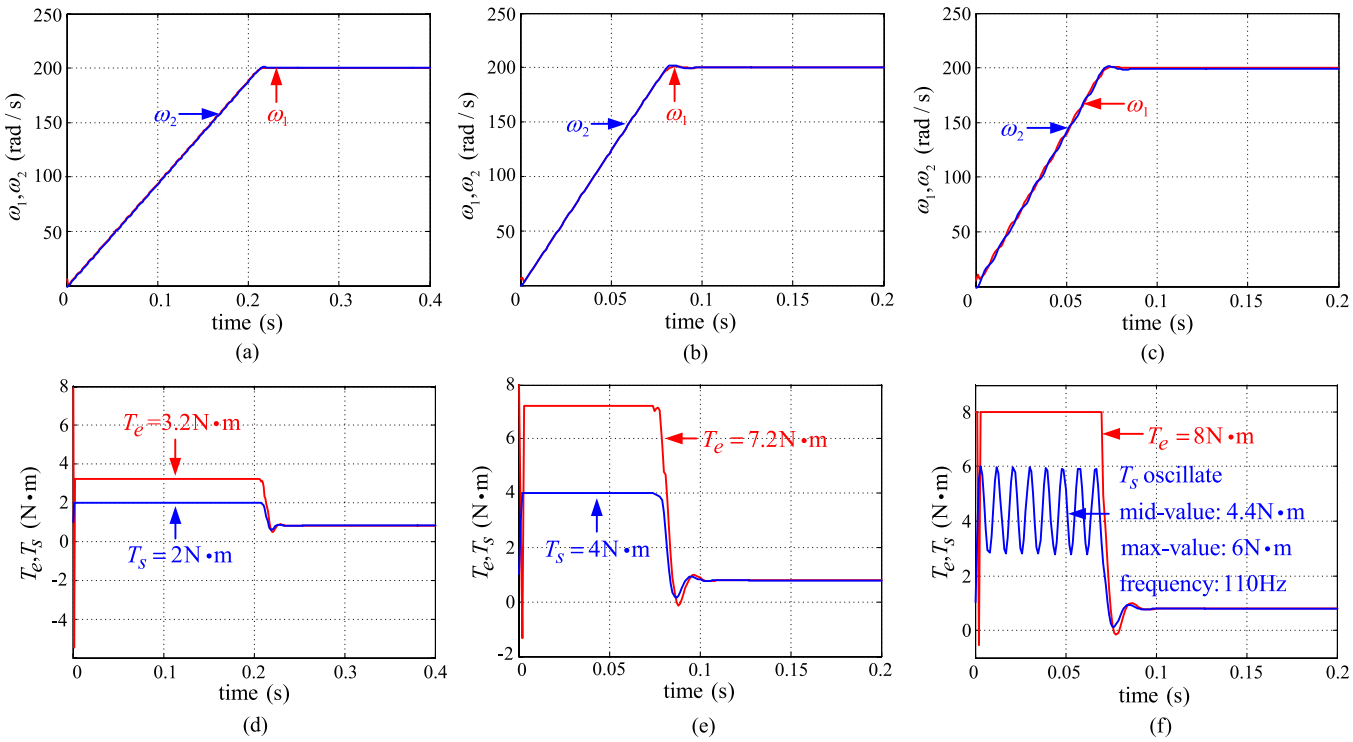

Fig. 6. Simulation results of speed and torque step response based on EMPC. (a)–(c). Motor speed and load speed. (d)–(f) Electromagnetic torque and shaft torque. (a) and (d) $\overline{T}_s = 2$. (b) and (e) $\overline{T}_s = 4$. (c) and (f) $\overline{T}_s = 6$.

The desired closed-loop performance can be achieved by manipulating the values of the input and state weighting matrices R and Q. The state weight can also be transferred to the output weighting, which can be set as follows:

$$Q = C^T Q_y C \quad Q_y = \begin{bmatrix} 3 & 0 \\ 0 & 0.5 \end{bmatrix} \quad R = 2 \times 10^{-4}. \tag{13}$$

The EMPC controller computed with MPT toolbox returns a solution of the polyhedral regions and the associated affine control laws defined on a 5-dimensional state space partition.

Simulation studies working with the EMPC controller are conducted by MATLAB/Simulink and the parameters are shown in Table II. The reference value is set to 100% of the nominal speed (200 rad/s); electromagnetic torque is selected two times of the nominal torque; the load torque of friction type during operation is 0.8 N·m.

The simulation results where the shaft torque constraint is set to be 2 N·m, 4 N·m, and 6 N·m, respectively, which can be shown in Fig. 6. Theoretically, the system with EMPC controller ensures free configuration of the closed-loop poles location, so does the design of mechanical characteristics.

As shown in Fig. 6(a) and (d), due to the tighter bound on the shaft torque variable as the case of 2 N·m, it decreases much faster in order to maintain the shaft torque response within the safe region. The tighter the shaft torque constraint is, the smaller the deviations between ω_1 and ω_2 will be. The electromagnetic torque and shaft torque both approach the horizontal line in two stages, namely the system provides maximum acceleration to keep the motor and load speed basically follow the set-points and ensure a perfect dynamic performance of the system.

Then, the drive system with a bigger value of shaft torque constraint as 4 N·m is tested in Fig. 6(b) and (e), which indicate a faster dynamic performance. On the basis of perfect vibration suppression, the system can show good dynamic characteristics.

IV. Critical Value for Shaft Torque Limitation Control

Due to the ultimate goal of speed control in the two-mass drive system is speed tracking, i.e., $\omega_2 \to \omega_1$, $d\omega_2/dt \to d\omega_1/dt$, the following relationship between the electromagnetic torque and shaft torque should be naturally formulated:

$$\frac{1}{J_1}\int_0^t (T_e - T_s)dt = \frac{1}{J_2}\int_0^t (T_s - T_L)dt \tag{14}$$

$$\frac{1}{J_1}(T_e - T_s) = \frac{1}{J_2}(T_s - T_L). \tag{15}$$

Furthermore, the two equations aforementioned can be rewritten as the simplified form, where R represents the inertia ratio between the load and the motor

$$T_e = \frac{R+1}{R}T_s - \frac{1}{R}T_L \tag{16}$$

$$R\int_0^t (T_e - T_s)dt = \int_0^t (T_s - T_L)dt. \tag{17}$$

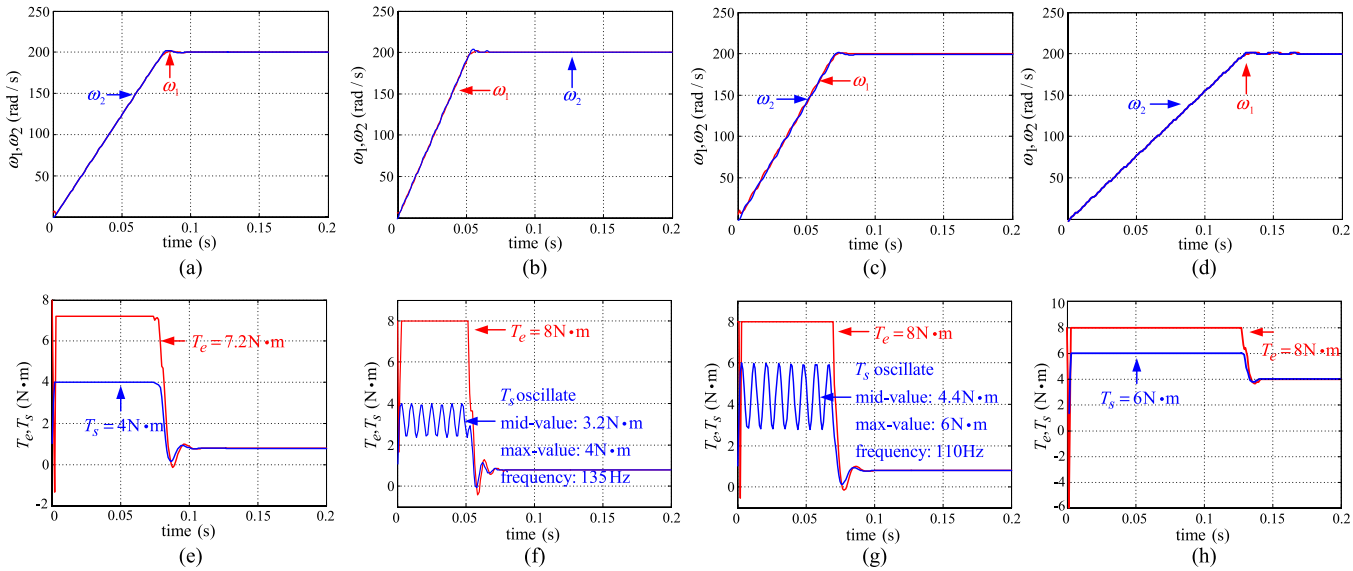

Fig. 7. Simulation transients of the two-mass system. (a)–(d) Motor and load speeds. (e)–(h) Electromagnetic and shaft torques. (a) and (e) For the case of $R = 1$, $T_L = 0.8$, $\overline{T}_s = 4$. (b) and (f) For the case of $R = 0.5$, $T_L = 0.8$, $\overline{T}_s = 4$. (c) and (g) For the case of $R = 1$, $T_L = 0.8$, $\overline{T}_s = 6$. (d) and (h) For the case of $R = 1$, $T_L = 4$, $\overline{T}_s = 6$.

The corresponding relationship between the electromagnetic and shaft torque is given as (16), and particularly, when the load inertia is equivalent to the motor inertia, together with the ignored disturbance torque, the simplified proportional relation formula is emerges

$$T_e = 2T_s. \tag{18}$$

Since the ultimate goal of the EMPC algorithm is to achieve both the speed tracking and the shaft torque limitation control, it makes this strategy explicitly incorporate the corresponding state constraints into control problem formulation. Unfortunately, it will certainly bring constraints to the theoretical deduction (16), and coincidentally meet with (17) as a geometric relationship practically. Hence, the following conclusion is derived:

$$\begin{cases} T_e = \frac{R+1}{R}T_s - \frac{1}{R}T_L & \text{if } \overline{T}_s \le \frac{R\cdot\overline{T}_e+T_L}{R+1} \\ T_s \text{ oscillate at} & \\ \text{mid-value: } \frac{R\cdot\overline{T}_e+T_L}{R+1} & \text{if } \overline{T}_s > \frac{R\cdot\overline{T}_e+T_L}{R+1} \\ \text{max-value: } \overline{T}_s & \\ \text{frequency: } f_{NT} & \end{cases} \tag{19}$$

where f_{NT} is the natural torsional frequency in the two-mass elastic system.

Conclusively, the time-domain response of the electromagnetic torque and shaft torque should satisfy (16) and (17) simultaneously, to complete the expressed speed tracking and shaft torque limitation control required by the system.

The corresponding response of electromagnetic torque and shaft torque can be deduced from formula (19), which is exactly the same with the result in Fig. 6. When $\overline{T}_s$ is smaller than the critical value of shaft torque, the amplitude limiting function can be guaranteed, which are shown in Fig. 6(d) and (e). When $\overline{T}_s$ is bigger than the critical value of shaft torque, shaft torque response will oscillate with the critical value 4.4 N·m as the mid-value, the preset shaft torque limit 6 N·m as the max-value and the natural torsional frequency 110 Hz as the oscillation frequency. However, the amplitude limiting function is still available, which is shown in Fig. 6(f).

The critical value of shaft torque deduced from formula (19) is calculated by R, T_L, and $\overline{T}_e$. It is also firmly concluded that the critical value of shaft torque varies with the inertia ratio and load torque. If the inertia ratio or the load inertia increases, the critical value will also be enhanced, as the result of the widened range of the shaft torque limitation. Thus, the impact of R and T_L within shaft torque amplitude limiting constraints is further verified in Fig. 7.

The impact of inertia ratio R on the critical value of shaft torque is first studied in the condition of $\overline{T}_s = 4$. When $R = 1$, $T_L = 0.8$, it can be deduced from formula (19) that the critical value of shaft torque is 4.4 N·m, which is bigger than the preset value 4 N·m. The shaft torque will output the amplitude limiting value, which exactly matches the simulation in Fig. 7(e). After the inertia ratio is decreased to $R = 0.5$, it can be deduced from formula (19) that the critical value of shaft torque is 3.2 N·m which is smaller than the preset value, thus the shaft torque will oscillates. Theoretical deductions are exactly matched with the simulations in Fig. 7(f).

Then the impact of load torque T_L to critical value of shaft torque is studied in the condition of $\overline{T}_s = 6$. When the relatively small T_L which is 0.8 is considered in Fig. 7(g), it can be seen that the output of shaft torque oscillates. However, when T_L increases to 4, the relationship between the critical value of shaft torque and the preset shaft amplitude limiting value will change and the shaft torque without oscillation will appear which is shown in Fig. 7(h). The results shown in Fig. 7 are in full accordance with the constraint condition of shaft torque amplitude limiting as formula (19).

TABLE I
RELATIONSHIP BETWEEN PREDICTION HORIZON AND THE SIZE OF CONTROL DATA FILE

N_u and N_p	The data file size of the control law
N_u=3, N_p=14	2.8 Mb
N_u=3, N_p=5	1.9 Mb
N_u=2, N_p=3	311 Kb
N_u=1, N_p=2	32 Kb
N_u=1, N_p=1	24 Kb

V. EMPC-PI SWITCHING CONTROL

A. Detection of Online Computing Time and the Size of Control Data File of EMPC

For purpose of the successful application of the EMPC controller in typical drives, first, its online computing time should be tested. The parameters of the controller are designed as $\overline{T}_e = 8$ N · m, $\overline{T}_s = 4$ N · m, $N_u = 1$, $N_p = 2$. The current loop break period of the simple PI vector control without the EMPC controller, and with the EMPC program should be detected, respectively. Low level represents DSP is in the break period. The tested results confirm the time delay of 40 us is the online EMPC controller computation time, which can be achieved in a current loop within 100 us sampling period.

To solve the problem of large amount of data storage space occupied by the EMPC controller, the prediction and control horizon N_p and N_u should be properly reduced, and thus the compressed data of the controller can be stored in the control unit. However, as the prediction step decreases, the transient control effect of the EMPC controller can be maintained, once the motor speed accesses to a given steady state, each state of the system will significantly oscillates. The smaller the prediction horizon is, the more intense oscillations will occur, until the controller completely loses its control ability. Table I gives the relationship between the prediction horizon and the data file size of the control law, under the condition of $\overline{T}_e = 8$ N · m, $\overline{T}_s = 4$ N · m, $\omega_r = 200$ rad/s. The data files of the EMPC law is generated by the MATLAB-MPT toolbox.

Because of the experimental hardware platform employed the TI's DSP-TMS320F28335 without any external expansion memories, whose programmable RAM is only 64 Kb, only the condition of $N_u = 1$, $N_p = 2$ can be chosen in the experiment.

B. Switching Criterion of EMPC-PI Switching Control

In order to verify the function of amplitude limiting control of EMPC, the effect of PI controller is simulated first. The parameters of PI controller are designed by pole placement with the same damping coefficient due to its widely application of inertia ratio [5]. Two-mass elastic system can be considered as a four-order system, and its poles can be expressed as two pairs of conjugate poles. As shown in Fig. 8, the pole damping coefficients are all set to be 0.5 and the distribution of poles is on the complex imaginary lines with 30 degrees to the negative real axis. Then the designed parameters of PI controller are $K_p = 1.24$, $K_i = 245.04$. In addition, the integral effect of PI controller will bring in windup phenomenon to the system which is solved by linear antitracking computational method [27]–[29].

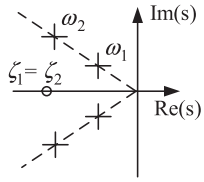

Fig. 8. Poles distribution of the two-mass elastic system using pole placement method with identical damping coefficient.

The simulation results are shown in Fig. 9(a) and (e). As expected in Fig. 9(a) and (e), although the traditional optimized PI control can ensure the system eventually converge, the oscillation is still relatively significant and the speed difference between the motor and load is clearly visible in the presence of the transient operation, and also brings about the risk of system safety when the shaft torque response exceeds its tolerance range. The fundamental reason comes from the fact that the two-mass elastic system as a four-order system with only two adjustable PI parameters to configure the poles of the system makes the system fail to meet the optimal performance.

Then, the simulations without considering attainable actual practice are given in Fig. 9(b) and (f), with the bigger prediction horizon as $N_p = 14$ and $N_u = 3$. Theoretically, the EMPC algorithm is already excellent enough to achieve the performance of vibration suppression and shaft torque safety.

When the problem of hardware implementation is considered, a smaller prediction horizon should be used to satisfy the narrow data storage ability of DSP-TMS320F28335. $N_u = 1$, $N_p = 2$ is designed in the EMPC controller, with the simulations shown in Fig. 9(c) and (g), and the expected poor steady state performance with continuous oscillation can be seen.

Thus, the EMPC-PI switching control was first proposed in this paper, which is committed to apply shaft torque amplitude limiting function of EMPC in speed transient into typical drives. The conventional PI controller is employed in speed steady state. Based on its integral function to errors, it is capable of realizing a commendable zero static error, whereas the EMPC cannot achieve.

The switching criterion of EMPC-PI switching control is based on the speed hysteresis value and hysteresis range. The range of hysteresis speed is chosen as $|\omega_1 - \omega_r| \leq \alpha\omega_r$ and the speed hysteresis value is $(\alpha\omega_r)$, where α refers to the hysteresis coefficient, which can be adjusted properly under different circumstances. In this paper, the coefficient α was set to be 2%. When the motor speed is within the range of $|\omega_1 - \omega_r| \leqslant \alpha\omega_r$, the speed enters the steady state and the PI controller will be implemented. Once the motor speed is beyond this hysteresis range, the speed is deemed to be within the transient state and the EMPC controller will be implemented.

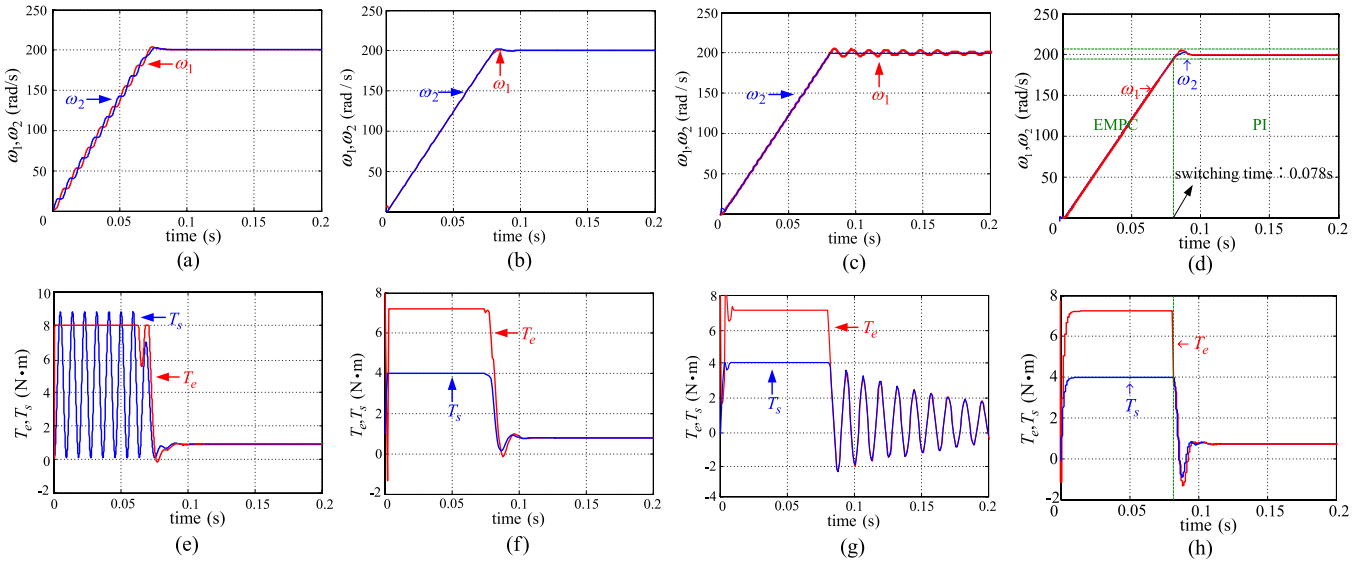

Fig. 9. Simulation transients of speed and torque step response with four control methods. (a) and (e) PI control. (b) and (f) EMPC control ($N_p = 14$, $N_u = 3$). (c) and (g) EMPC control ($N_p = 2$, $N_u = 1$). (d) and (h) EMPC-PI switching control.

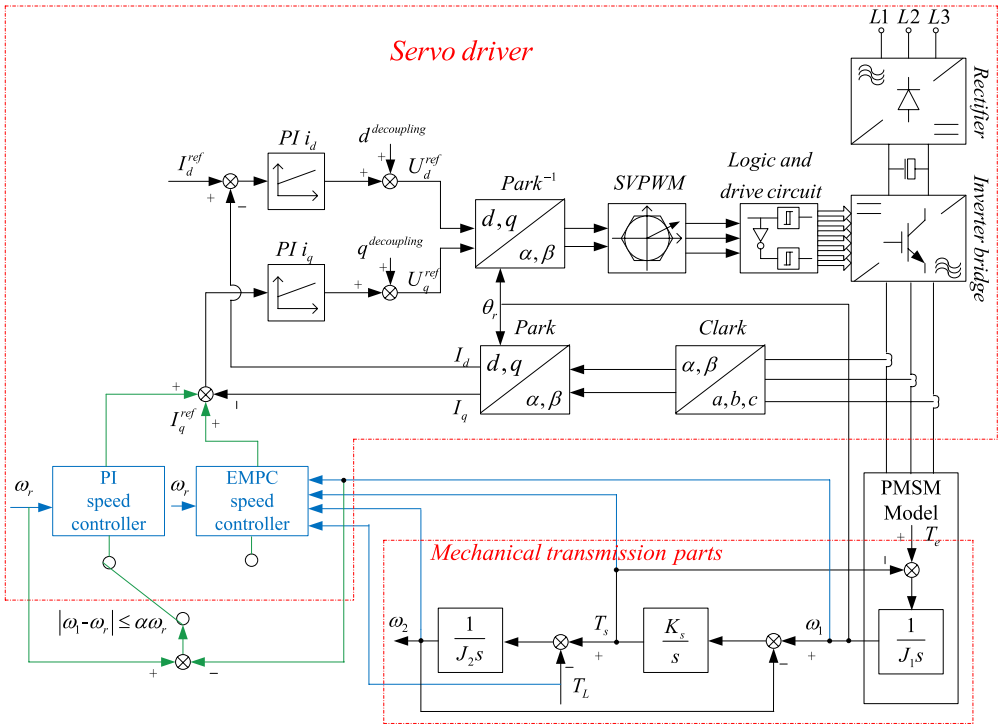

Fig. 10. Structure diagram of the integral servo system with the EMPC-PI controller.

The structure diagram of the integral servo system with the EMPC-PI controller is shown in Fig. 10.

The simulations shown in Fig. 9(d) and (h), demonstrate the EMPC-PI switching controller can ensure desired control effect during both transient and steady process, and solve the problem of excessive data storage as well. In contrast to the dSPACE hardware used in [16]–[23], this optimal control performance can be successfully implemented using a conventional DSP (TMS320F28335) with this strategy, closer to the actual industrial applications.

In order to verify the effectiveness of EMPC-PI switching control, the results of some special states: time variant reference speed as sinusoidal reference speed signal and step change of load torque at constant speed are added as shown in Fig. 11.

The speed and torque responses are shown in Fig. 11(a) and (c), where the reference signal is a sine wave with 5 Hz as its frequency and 100 rad/s as its amplitude. The step responses of a sudden 50% load torque added at 0.15 s are shown in Fig. 11(b) and (d).

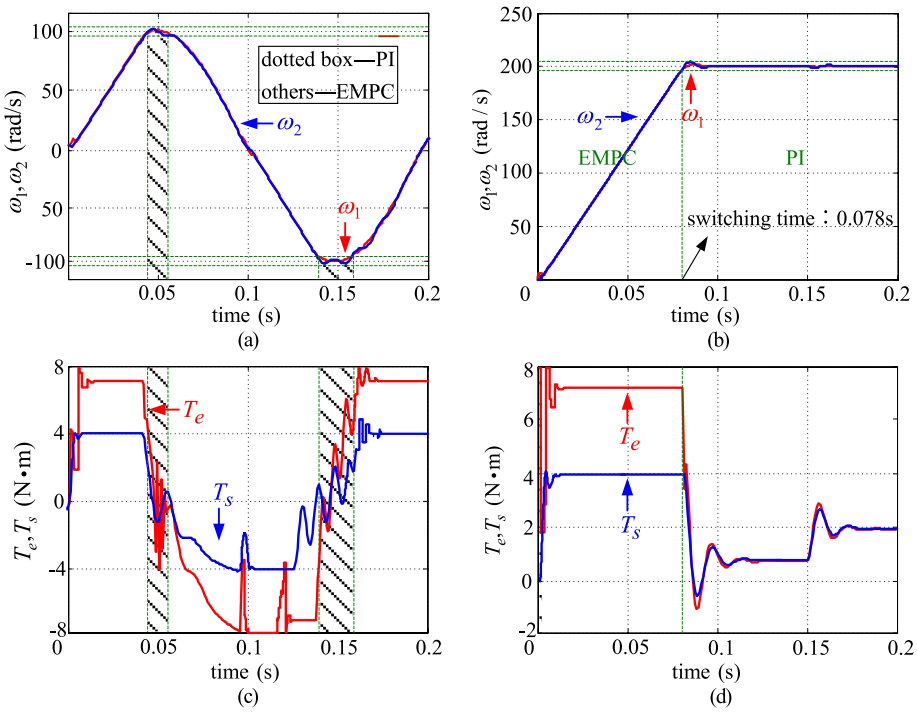

Fig. 11. Simulation transients of the two-mass system. (a) and (b) Motor and load speeds. (c) and (d) Electromagnetic and shaft torques. (a) and (c) For the case of sinusoidal reference speed signal. (a) and (c) Step change of load torque at constant speed (b) and (d).

The whole switching procedure of EMPC-PI in the two-mass system is fully manifested in two different situations. The switching moment has been marked in Fig. 11, which demonstrates the favorable switching performance of EMPC-PI controller under different operating states. EMPC-PI controller can realize the torque amplitude limiting in transient state, whereas zero steady-state error tracking in steady state.

C. Robust Analysis of EMPC-PI Switching Control

The system robustness has been studied in this paper in the condition that the shaft stiffness and load inertia within the system model are different from the designed EMPC controller.

Robustness of the proposed EMPC-PI controller to variations in drive parameters used in the controller synthesis procedure is examined [30], [31]. The effect of uncertainty in the value of shaft stiffness is shown in Fig. 12(b) and (f) and Fig. 12(c) and (g) for $K_s = 0.5 * K_{sN}$ and $K_s = 2 * K_{sN}$, respectively. As can be seen from the results, the speed and torque transients are slightly different from the case with the normal system parameters previously mentioned in Fig. 10(d) and (g). However the safety constraint on the shaft torque is not violated. It means that the designed system is robust against the variation in K_s.

The performance of the drive systems subject to changes in the load inertia is presented in Fig. 12(c), (d), (g), and (h). It is clear that although the variation of these parameters has a significant impact on the dynamic response of the drive system, the control structure protects the maximal tension limit of the motor and shaft thus guaranteeing safe operation of the drive.

VI. Experimental Results

The laboratory setup, which is presented in Fig. 13, is composed of two Siemens-1FL5060-0AC21-0AG0 PMSM motors (as the driver and load machines), 750W driver with TMS320F28335 DSP control board. The two motors are coupled by a Helical-MC7CM200 elastic coupling. The load motor functions as not only an inertia load, but also adding load torque. The dc buses of the driver motor and the load motor are in parallel connection and the load motor is used as a generator to supply the load torque. A 20% of the rated torque is added in simulations and experiments in this paper. The main parameters are presented in Table II.

The experimental results that can prove the effectiveness of EMPC-PI control are demonstrated in Figs. 14 and 15.

In Fig. 14, the effectiveness of EMPC-PI switching control is verified with the results of some special states, similarly as in simulation tests as Fig. 11. The hysteresis coefficient α is chosen as 10% in Fig. 14(a) and 20% in Fig. 14(b) and (d) for the practical factors. The simulation study is supported by experimental results, further demonstrating the favorable switching performance of EMPC-PI controller under different operating states. EMPC-PI controller can realize the torque amplitude limiting in transient state, whereas zero steady-state error tracking in steady state. However, it is also shown from Fig. 14(c) that within the switching range, the responses of the electromagnetic torque and shaft torque are not smooth, which can be deeply studied in the future.

In Fig. 15(a) and (e), experimental results of the PI controller designed by pole placement with the same damping coefficient, similarly as in simulation tests are presented, where the PI

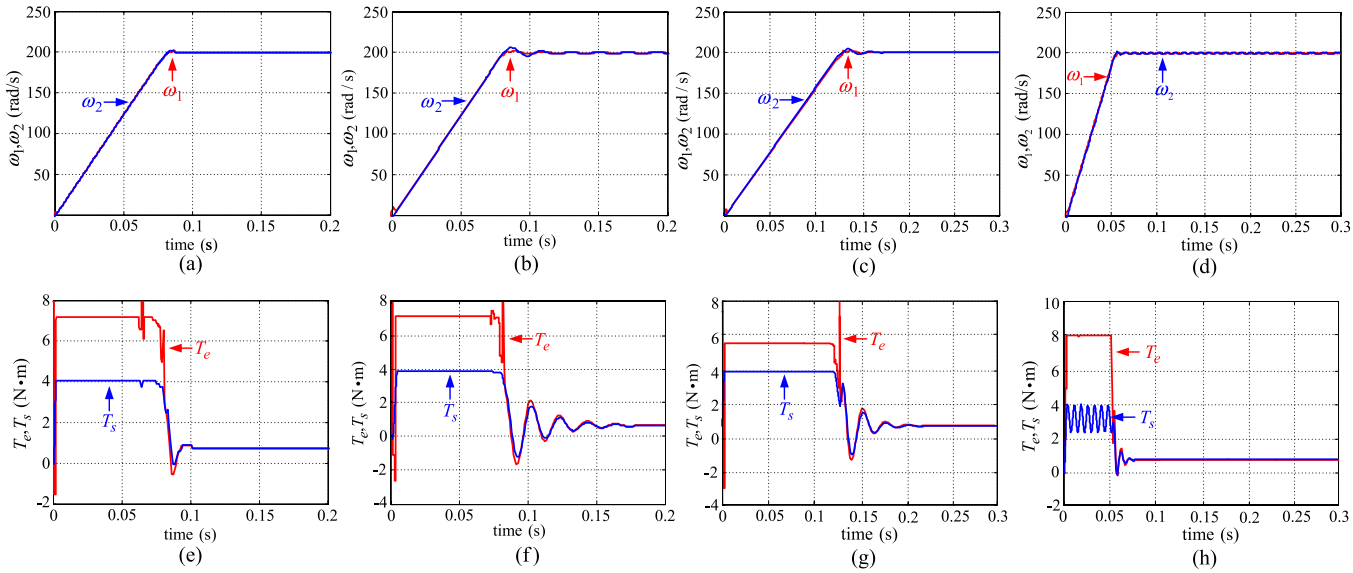

Fig. 12. Simulation transients of the two-mass system. (a)–(d) Motor and load speeds. (e)–(h) Electromagnetic and shaft torques. (a) and (e) For the case of changed the shaft stiffness $K_s = 2 * K_{sN}$. (b) and (f) $K_s = 0.5 * K_{sN}$. (c) and (g) for the case of changed the inertia of the load machine $J_2 = 2 * J_{2N}$. (d) and (h) $J_2 = 0.5 * J_{2N}$.

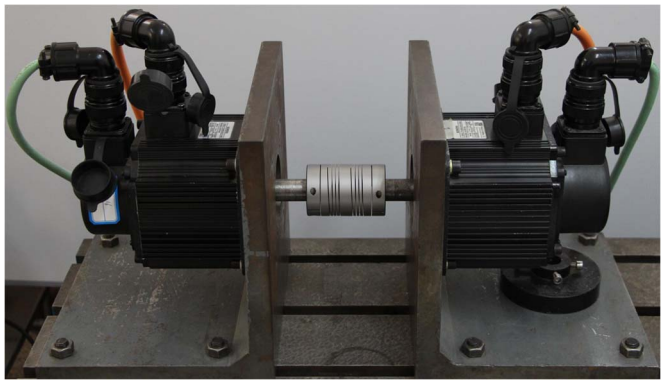

Fig. 13. Photograph of the experimental setup.

TABLE II
MAIN PARAMETERS OF PMSM DRIVE SYSTEM

parameter	nominal value
Motor Power	750W
Motor Torque	4 N·m
Motor Speed	200 rad/s
Inertia of motor	1.27e-3 N·m^2
Inertia of load	1.27e-3 N·m^2
Stiffness of elastic coupling	305 N·m/rad
Non-reversing torque of coupling	13 N·m
Shock ro reserving torque of coupling	6.4 N·m
Momentary torque of coupling	26 N·m
Anti-resonance frequency	78.4 Hz
Resonance frequency	110 Hz

controller is unable to keep both the shaft torque response within the safety bound and stable state. The experimental results correspond with different shaft torque constraints are presented in Fig. 15 [excluded (a) and (e)], as can be concluded from which, all the responses clearly demonstrate the potential of the EMPC-PI in perfect control effect of the vibration suppression, any level of the motor and shaft torque limitation together with the optimal and fast dynamic in the typical drive.

The experimental results that can prove the robustness of EMPC-PI control in the condition of changed shaft stiffness and load inertia within the system model are demonstrated in Fig. 16, which are similar as simulation situations. It is clear that although the variation of these parameters has a significant impact on the dynamic response of the drive system, the control structure protects the maximal tension limit of the motor and shaft thus guaranteeing safe operation of the drive.

Meanwhile, the constraints for shaft torque limit conditions can be verified totally met with the system response in all the experimental results, as shown in Figs. 14–16.

When $\overline{T}_s$ is smaller than the critical value of shaft torque, the amplitude limiting function can be guaranteed, which is shown in Figs. 14(d), 15(f), (g), and 16(e)–(g). When $\overline{T}_s$ is bigger than the critical value of shaft torque, shaft torque response will oscillates but the amplitude limiting function is still available which is shown in Figs. 15(h) and 16(h).

All theoretical considerations and simulations are confirmed experimentally.

VII. CONCLUSION

In this paper, mechanical oscillations and safety issues of the shaft are overcome by focusing on the theoretical analyses and design process of MPC strategy. According to MPC

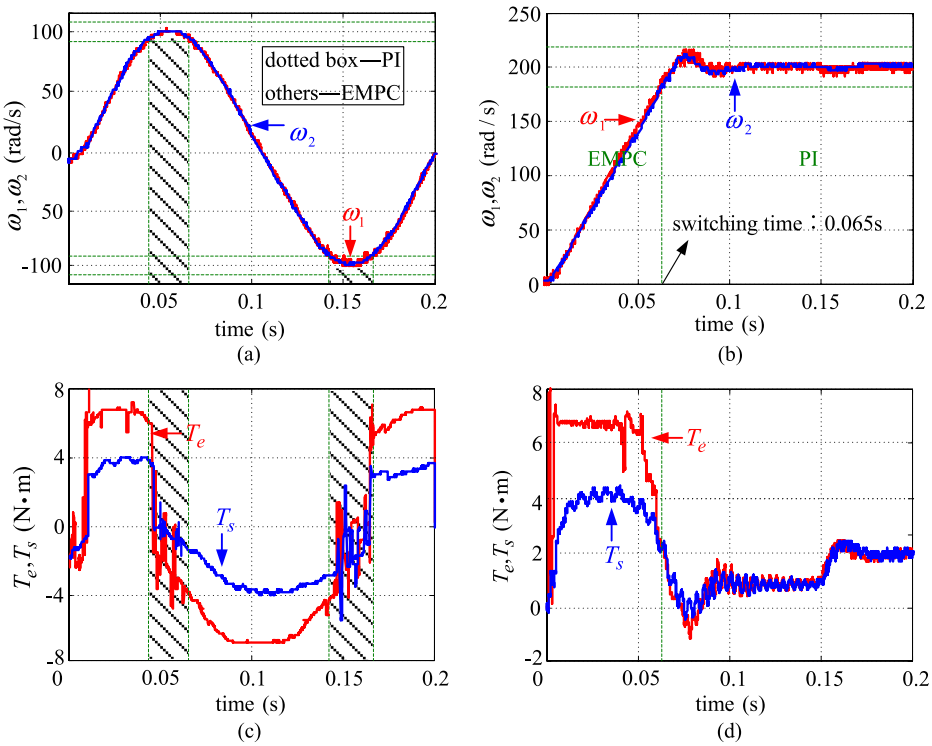

Fig. 14. Experimental transients of the two-mass system. (a) and (b) Motor and load speeds, electromagnetic, and shaft torques. (c) and (d) For the case of sinusoidal reference speed signal. (a) and (c) Step change of load torque at constant speed (b) and (d).

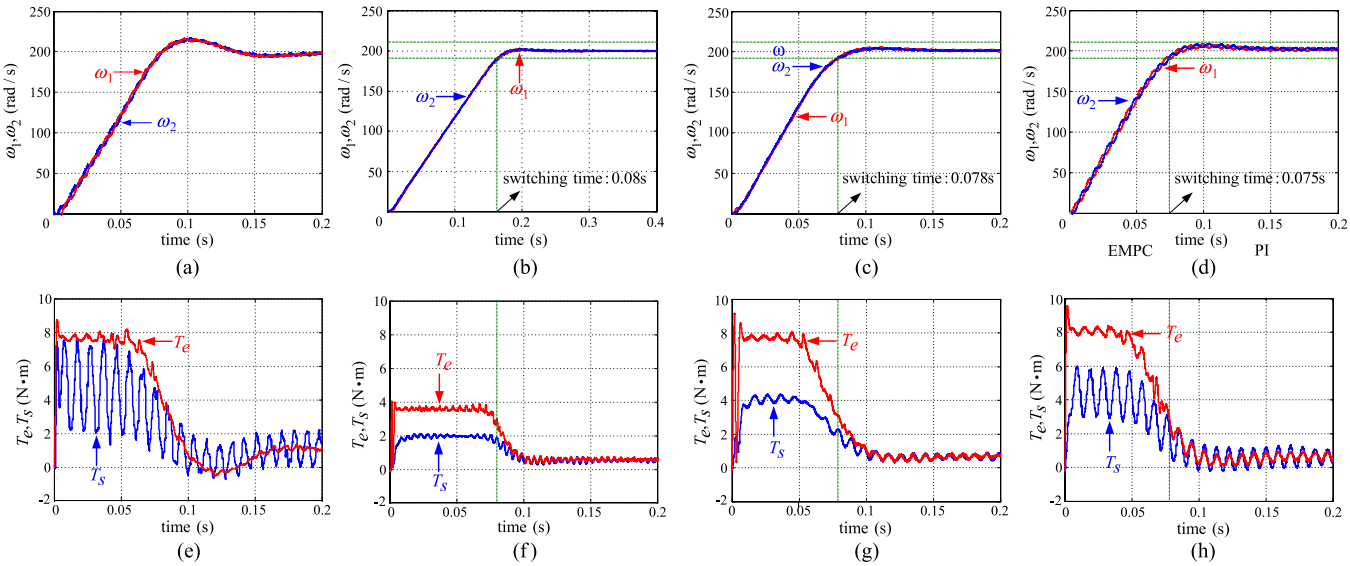

Fig. 15. Experimental results of speed and torque step response. (a) and (e) PI control. (b)and (f) EMPC-PI control $(\overline{T}_s = 2)$ (c) and (g) EMPC-PI switching control $(\overline{T}_s = 4)$ (d) and (h) EMPC-PI switching control with $(\overline{T}_s = 6)$.

optimization with constraints principle, two-step prediction is used. Then conventional MPC is simplified as the fast EMPC to reduce the amount of online computing, with the ultimate implementation of the EMPC-PI switching control in the typical drive. The constraint condition of shaft torque limitation control is presented in the system, showing the oscillations will appear on the basis of the guaranteed limitation control when the preset shaft torque limit is larger than the theoretical critical value. And change the critical value of shaft torque varies with the inertia ratio and load torque. The amount of online computation can be significantly reduced using EMPC-PI switching, where the switching criterion is based on the speed difference hysteresis value. The control method can suppress mechanical resonance, limit the amplitude of shaft torque, and it is also robust against changed parameters, thus providing desired dynamic performance.

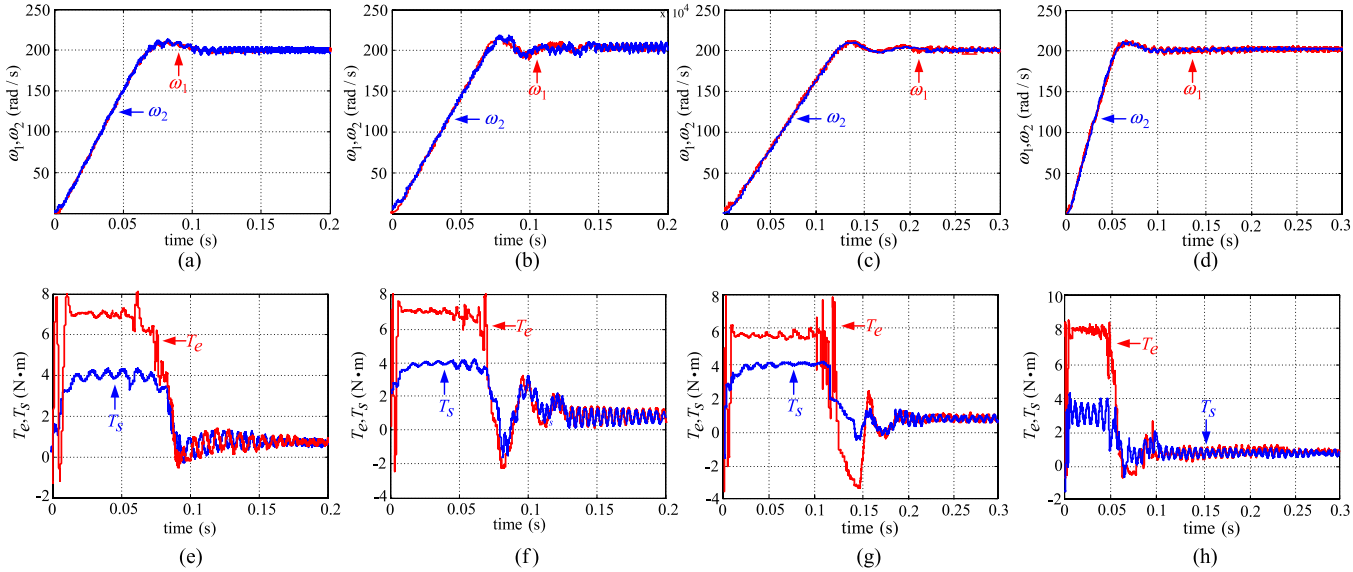

Fig. 16. Experimental results of the two-mass system. (a)–(d) motor and load speeds. (e)–(h) Electromagnetic and shaft torques. (a) and (e) For the case of changed the shaft stiffness $K_s = 2 * K_{sN}$. (b) and (f) $K_s = 0.5 * K_{sN}$. (c) and (g) For the case of changed the inertia of the load machine $J_2 = 2 * J_{2N}$. (d) and (h) $J_2 = 0.5 * J_{2N}$.

Further work will focus on the resolute strategy's exploration for the constraint condition of shaft torque limitation control, which will extend the shaft torque limit range.

REFERENCES

[1] M. A. Valenzuela, J. M. Bentley, and R. D. Lorenz, "Evaluation of torsional oscillations in paper machine sections," *IEEE Trans. Ind. Appl.*, vol. 41, no. 2, pp. 493–501, Mar./Apr. 2005.

[2] S. J. Qin and T. A. Badgwell, "A survey of industrial model predictive control technology," *Control Eng. Pract.*, vol. 11, no. 7, pp. 733–764, Jul. 2003.

[3] C. I. Kang and C. H. Kim, "An adaptive notch filter for suppressing mechanical resonance in high track density disk drives," *Microsyst. Technol.*, vol. 11, no. 8–10, pp. 638–652, May 2005.

[4] S. Katsura and K. Ohnishi, "Force servoing by flexible manipulator based on resonance ratio control," in *Proc. IEEE ISIE*, Jun. 2005, pp. 1343–1348.

[5] C. Wang, M. Yang, G. Wang, and D. Xu, "Mechanical resonance suppression and shaft torque limitation of two-mass drive system based on model predictive control," in *Proc. IEEE IECON*, Oct. 2014, pp. 2804–2809.

[6] S. Thomsen, N. Hoffmann, and F. W. Fuchs, "PI control, PI-based state space control, and model-based predictive control for drive systems with elastically coupled loads—A comparative study," *IEEE Trans. Ind. Electron.*, vol. 58, no. 8, pp. 3647–3657, Aug. 2011.

[7] K. Szabat and T. Orlowska-Kowalska, "Application of the Kalman filters to the high-performance drive system with elastic coupling," *IEEE Trans. Ind. Electron.*, vol. 59, no. 11, pp. 4226–4235, Nov. 2012.

[8] R. Dhaouadi, K. Kubo, and M. Tobise, "Two-degree-of-freedom robust speed controller for high-performance rolling mill drives," *IEEE Trans. Ind. Appl.*, vol. 29, no. 5, pp. 919–926, Sep./Oct. 1993.

[9] K. Peter, I. Schoeling, and B. Orlik, "Robust output-feedback H∞control with a nonlinear observer for a two-mass system," *IEEE Trans. Ind. Appl.*, vol. 39, no. 3, pp. 637–644, May/Jun. 2003.

[10] S. A. Davari, D. A. Khaburi, F. Wang, and R. M. Kennel, "Using full order and reduced order observers for robust sensorless predictive torque control of induction motors," *IEEE Trans. Power Electron.*, vol. 27, no. 7, pp. 3424–3433, Jul. 2012.

[11] T. Orlowska-Kowalska and K. Szabat, "Control of the drive system with stiff and slastic couplings using adaptive neuro-fuzzy approach," *IEEE Trans. Ind. Electron.*, vol. 54, no. 1, pp. 228–240, Jan./Feb. 2007.

[12] K. Szabat and T. Orlowska-Kowalska, "Performance improvement of the industrial drives with mechanical elasticity using nonlinear adaptive Kalman filter," *IEEE Trans. Ind. Electron.*, vol. 55, no. 3, pp. 1075–1084, Mar. 2008.

[13] M. Vasak and N. Peric, "Protective predictive control of electrical drives with elastic transmission," in *Proc. Power Electron. Motion Control Conf.*, Sep. 2008, pp. 2235–2240.

[14] M. Vasak, N. Peric, K. Szabat, and M. Cychowski "Patched LQR control for robust protection of multi-mass electrical drives with constraints," in *Proc. IEEE ISIE*, Jul. 2010, pp. 3153–3158.

[15] E. Fuentes, D. Kalise, J. Rodriguez, and R. M. Kennel, "Cascade-free predictive speed control for electrical drives," *IEEE Trans. Ind. Electron.*, vol. 61, no. 5, pp. 2176–2184, May 2014.

[16] S. Bolognani, L. Peretti, and M. Zigliotto, "Combined speed and current model predictive control with inherent field-weakening features for PMSM drives," in *Proc. 14th IEEE MELECON*, 2008, pp. 472–478.

[17] S. C. Carpiuc and C. Lazar, "Lyapunov-based constrained explicit current predictive control in permanent magnet synchronous machine drives," in *Proc. IEEE SPEEDAM*, Jun. 2014, pp. 461–466.

[18] M. Cychowski, K. Szabat, and T. Orlowska-Kowalska, "Constrained model predictive control of the drive system with mechanical elasticity," *IEEE Trans. Ind. Electron.*, vol. 56, no. 6, pp. 1963–1973, Jun. 2009.

[19] M. Cychowski, C. Do, P. Serkies, and K. Szabat, "Position tracking in electrical drives with elastic coupling using model predictive control," in *Proc. IEEE IECON*, Nov. 2010, pp. 956–961.

[20] S. Bolognani, L. Peretti, and M. Zigliotto, "Design and implementation of model predictive control for electrical motor drives," *IEEE Trans. Ind. Electron.*, vol. 56, no. 6, pp. 1925–1936, Jun. 2009.

[21] K. Szabat, P. Serkies, T. Orlowska-Kowalska, and M. Cychowski, "Robust torque constraints handling in drive systems with elastic transmission," in *Proc. IEEE ICIT*, Mar. 2010, pp. 398–403.

[22] K. Szabat, P. Serkies, and M. Cychowski, "Application of the MPC to the robust control of the two-mass drive system," in *Proc. IEEE ISIE*, Jun. 2011, pp. 1901–1906.

[23] M. T. Cychowski and K. Szabat, "Efficient real-time model predictive control of the drive system with elastic transmission," *IET Control Theory Appl.*, vol. 4, no. 1, pp. 37–49, Jan. 2010.

[24] P. Serkies, T. Orlowska-Kowalska, M. Cychowski, and K. Szabat, "Robust model predictive speed control of the drive system with an elastic joint," in *Proc. IEEE EUROCON–Int. Conf. Comput. Tool*, 2011, pp. 1–4.

[25] P. J. Serkies and K. Szabat, "Application of the MPC to the position control of the two-mass drive system," *IEEE Trans. Ind. Electron.*, vol. 60, no. 9, pp. 3679–3688, Sep. 2013.

[26] J. Bocker, B. Freudenberg, A. The, and S. Dieckerhoff, "Experimental comparison of model predictive control and cascaded control of the modular multilevel converter," *IEEE Trans. Power Electron.*, vol. 30, no. 1, pp. 422–430, Jan. 2015.

[27] K. J. Aström and T. Hägglund, *PID Controllers: Theory, Design and Tuning*. Research Triangle Park, NC, USA: ISA, 1995.

[28] D. Zhang, H. Li, and E. G. Collins, "Digital anti-windup PI controllers for variable-speed motor drives using FPGA and stochastic theory," *IEEE Trans. Power Electron.*, vol. 21, no. 5, pp. 1496–1501, Sep. 2006.
[29] S. Wang, W. Zhu, S. Huang, and F. Hou, "Anti-windup speed regulator based on model predictive control," in *Proc. 17th ICEMS*, Oct. 2014, pp. 544–548.
[30] A. A. Zaki Diab, D. A. Kotin, V. N. Anosov, and V. V. Pankratov, "A comparative study of speed control based on MPC and PI-controller for indirect field oriented control of induction motor drive," in *Proc. 12th APEIE*, Oct. 2014, pp. 728–732.
[31] A. Damiano, G. Gatto, I. Marongiu, A. Perfetto, and A. Serpi, "Operating constraints management of a surface-mounted PM synchronous machine by means of an FPGA-based model predictive control algorithm," *IEEE Trans. Ind. Informat.*, vol. 10, no. 1, pp. 243–255, Feb. 2014.

Can Wang received the B.S. degree in electrical engineering from Harbin University of Science and Technology, Harbin, China, in 2012 and the M.S. degree in power electronics and electrical drives from Harbin Institute of Technology, Harbin, in 2014. She is currently working toward Ph.D. degree in power electronics and electrical drives in the School of Electrical Engineering and Automation, Harbin Institute of Technology.

Her current research interests include PMSM servo systems and mechanical resonance suppression.

Ming Yang (M'14) received the B.S., M.S., and Ph.D. degrees in electrical engineering from Harbin Institute of Technology (HIT), Harbin, China, in 2000, 2002, and 2007, respectively.

In 2004, he joined the Department of Electrical Engineering, HIT as a Lecturer, where he has been an Associate Professor of electrical engineering since 2010. From 2009 to 2012, he was a Postdoctoral Fellow with Shanghai STEP Electric Corporation. He has authored more than 40 technical papers published in journals and conference proceedings. He is the holder of 14 Chinese patents. His current major research interests include PMSM servo systems, predictive current control, and mechanical resonance suppression.

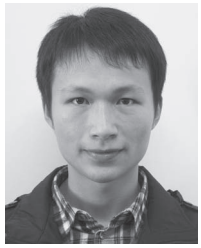

Weilong Zheng received the B.S. degree in electrical engineering from Harbin Institute of Technology, Harbin, China, in 2014, where he is currently working toward the M.S. degree in power electronics and electrical drives in the School of Electrical Engineering and Automation.

His current research interests are in PMSM servo systems and mechanical resonance suppression.

Jiang Long received the B.S. degree in electrical engineering and automation in 2012 from Chang Chun Institute of Technology, Chang Chun, China, and the M.S. degree in power electronics and electrical drives in 2015 from Harbin University of Science and Technology, Harbin, China, where he is currently working toward Ph.D. degree in power electronics and electrical drives in the School of Electrical Engineering and Automation.

His current research interests include PMSM servo system.

Dianguo Xu (M'97–SM'12) received the B.S. degree in control engineering from Harbin Engineering University, Harbin, China, in 1982, and the M.S. and Ph.D. degrees in electrical engineering from Harbin Institute of Technology (HIT), Harbin, in 1984 and 1989, respectively.

In 1984, he joined the Department of Electrical Engineering, HIT as an Assistant Professor. Since 1994, he has been a Professor with the Department of Electrical Engineering, HIT. He was the Dean of School of Electrical Engineering and Automation, HIT, from 2000 to 2010. He is currently the Vice President of HIT. His research interests include renewable energy generation technology, multiterminal HVDC systems based on VSC, power quality mitigation, and speed-sensorless vector-controlled motor drives. He has published over 600 technical papers.

Dr. Xu is an Associate Editor for the IEEE TRANSACTIONS ON INDUSTRIAL ELECTRONICS, and serves as Chairman of the IEEE Harbin Section.